Patch Clamp on the Luminal Membrane of Exocrine Gland Acini from Frog Skin (*Rana esculenta*) Reveals the Presence of Cystic Fibrosis Transmembrane Conductance Regulator–like Cl^- Channels Activated by Cyclic AMP

Jakob Balslev Sørensen and Erik Hviid Larsen

From the August Krogh Institute, University of Copenhagen, DK-2100 Copenhagen Ø, Denmark

ABSTRACT Chloride channels in the luminal membrane of exocrine gland acini from frog skin (*Rana esculenta*) constituted a single homogeneous population. In cell-attached patches, channels activated upon exposure to isoproterenol, forskolin, or dibutyryl-cAMP and isobutyl-1-methyl-xanthine rectified in the outward direction with a conductance of 10.0 ± 0.4 pS for outgoing currents. Channels in stimulated cells reversed at 0 mV applied potential, whereas channels in unstimulated cells reversed at depolarized potentials (28.1 ± 6.7 mV), indicating that Cl^- was above electrochemical equilibrium in unstimulated, but not in stimulated, cells. In excised inside-out patches with 25 mM Cl^- on the inside, activity of small (8-pS) linear Cl^--selective channels was dependent upon bath ATP (1.5 mM) and increased upon exposure to cAMP-dependent protein kinase. The channels displayed a single substate, located just below 2/3 of the full channel amplitude. Halide selectivity was identified as $P_{Br} > P_I > P_{Cl}$ from the Goldman equation; however, the conductance sequence when either halide was permeating the channel was $G_{Cl} > G_{Br} >> G_I$. In inside-out patches, the channels were blocked reversibly by 5-nitro-2-(3-phenylpropylamino)benzoic acid, glibenclamide, and diphenylamine-2-carboxylic acid, whereas 4,4-diisothiocyanatostilbene-2,2-disulfonic acid blocked channel activity completely and irreversibly. Single-channel kinetics revealed one open state (mean lifetime = 158 ± 72 ms) and two closed states (lifetimes: 12 ± 4 and 224 ± 31 ms, respectively). Power density spectra had a double-Lorentzian form with corner frequencies 0.85 ± 0.11 and 27.9 ± 2.9 Hz, respectively. These channels are considered homologous to the cystic fibrosis transmembrane conductance regulator Cl^- channel, which has been localized to the submucosal skin glands in *Xenopus* by immunohistochemistry (Engelhardt, J.F., S.S. Smith, E. Allen, J.R. Yankaskas, D.C. Dawson, and J.M. Wilson. 1994. *Am. J. Physiol.* 267: C491–C500) and, when stimulated by cAMP-dependent phosphorylation, are suggested to function in chloride secretion.

KEY WORDS: secretion • pharmacology • halide selectivity • rectification • DIDS

INTRODUCTION

With the advent of the patch-clamp technique, considerable effort has gone into the identification of the apical cAMP-dependent Cl^- channel involved in epithelial secretion. Three types are suggested to participate in cAMP-induced secretion: the outward rectifier Cl^- channel (shark rectal gland, Greger et al., 1987; colon carcinoma cells, Hayslett et al., 1987; airway cells, Frizzell et al., 1986), the small conductance 5–11-pS linear Cl^- channel (shark rectal gland, Gögelein et al., 1987; colon carcinoma cells, Hayslett et al., 1987; pancreatic ducts, Gray et al., 1989; airway cells, Frizzell et al., 1986; human tracheal gland, Becq et al., 1993*b*), and a population of very small conductance channels (<2 pS) (airway cells, Kunzelmann et al., 1994; and colon carcinoma cells, Fischer et al., 1992; Kunzelmann et al., 1992). Whereas it is generally accepted that the 5–11-pS channel is encoded by the cystic fibrosis transmembrane conductance regulator (CFTR)[1] gene, controversy remains on the identity and involvement of the other channels in secretion. The main interest in this subject derives from the disease cystic fibrosis, which is caused by mutation of the CFTR gene. Naturally, the identity and distribution of secretory Cl^- channels seems crucial for an understanding of the pathology of cystic fibrosis and for identification of redundant pathways that may aid in its therapy.

Due to the difficult anatomy of most secretory epithelia, in the majority of cases investigators must rely on

Address correspondence to Jakob Balslev Sørensen, August Krogh Institute, Universitetsparken 13, DK-2100 Copenhagen Ø, Denmark. Fax: +45 3532 1567; E-mail: JBSorensen@aki.ku.dk

[1]*Abbreviations used in this paper:* ANOVA, analysis of variance; CFTR, cystic fibrosis transmembrane conductance regulator; GHK, Goldman-Hodgkin-Katz; PDS, power density spectrum.

J. Gen. Physiol. © The Rockefeller University Press • 0022-1295/98/07/19/13 $2.00
Volume 112 July 1998 19–31
http://www.jgp.org

cultured cells, where the distribution of Cl^- channels or the expression of as yet unidentified subunits may be altered when compared with native tissue. An exception to this is the work done on freshly isolated shark rectal glands. However, being an osmoregulatory organ with specialized functions, the shark rectal gland may have a physiology that is not comparable with most isotonic secreting glands affected in cystic fibrosis.

Here we present a patch-clamp study of the luminal membrane of freshly isolated secretory gland acini from frog skin, which has been shown to be a major site for expression of CFTR in *Xenopus* (Engelhardt et al., 1994). The frog skin glands consist of numerous acini connected to the outside via very short ducts. They therefore present the interesting possibility of investigating primary acinar secretions almost unmodified by ductal activities. After adrenergic stimulation, the activity of the glands can be studied in isolation by blocking Na^+ absorption of the epithelium. Thus, the tissue has been used for the study of secretion using transepithelial electrical measurement combined with tracer studies (Koefoed-Johnsen et al., 1952; Thompson and Mills, 1983) and measurement of the water flow (Bjerregaard and Nielsen, 1987). Recently, a novel secretory model, the Na^+ recirculation model, was proposed for the frog skin glands (Ussing et al., 1996). The acini are easily isolated and the apical membrane can be patched after microdissection from the serosal side. We report that the only apical Cl^- channel found in this tissue is a 8–10 pS cAMP-regulated ion channel with properties similar, but not identical, to human CFTR. Properties of Na^+ channels found during the same investigation will be published elsewhere (see also Sørensen et al., 1998). Preliminary reports of this work have appeared (Sørensen and Larsen, 1998*a*, 1998*b*).

MATERIALS AND METHODS

Preparation of Isolated Epithelial Sheets

Frogs (*Rana esculenta*) were killed by decapitation and double pithing. The skin was dissected off in one piece and the connective tissue (corium) was removed by a combination of enzymatic and hydrostatic treatment (Andersen et al., 1995). In brief, the skin was mounted in a chamber exposing the mucosal side to a bath of NaCl Ringer thermostatically controlled at 29–30°C. The serosal side was treated with 1–1.2 mg/ml crude collagenase in NaCl Ringer for 75 min (Collagenase A; Boehringer-Mannheim GmbH, Mannheim, Germany, or Collagenase type 2; Worthington Biochemical Corp., Lakewood, NJ). A tube attached to the chamber was then filled with NaCl Ringer (the enzyme was not removed) to give an over-pressure of 10–25 cm H_2O on the serosal side. This treatment resulted in the detachment of the epithelium from the connective tissue in some areas. The skin was then transferred to a petri dish and the connective tissue was removed by gentle dissection from the serosal side, leaving a large area of epithelium intact. The epithelium was kept in aerated NaCl Ringer at room temperature (22–24°C) and used on the same day.

Preparation of Glands for Patch Clamp

A piece of the isolated epithelium was mounted in a chamber (area 0.79 cm^2, volume ~0.5 ml) against a coverslip with the serosal side up and placed on the stage of an inverted microscope (Zeiss IM35; Brock & Michelsen, Birkerød, Denmark). The serosal, but not the mucosal, side was perfused continuously (2–5 ml/min) with NaCl Ringer before and during seal formation, and perfusion persisted throughout the experiment in most cases. As viewed at low magnification (25×), the preparation consisted of an intact epithelial sheet with variable number of glands still attached, but stripped for connective tissue. The glands were viable as shown by trypan blue exclusion.

For patch clamp on the luminal side of the gland cells, the intact glands were microdissected from the serosal side using a discarded patch pipette (Fig. 1) under high magnification (400×). The pipette was shoved into the gland lumen and moved to either side to slit the gland acinus into two parts. In cases where this was difficult, the glands were softened by exposure to divalent cation-free Ringer (composition as NaCl Ringer but with 10 mM EGTA replacing $CaCl_2$ and $MgCl_2$) for ~5 min. The open gland acinus was pressed against and often adhered to the epithelium, exposing the luminal (apical) membrane. A new patch pipette could now be used for patch clamp of the luminal membrane. The firm attachment of the gland acinus to the duct and therefore to the epithelium made the use of a holding pipette superfluous and assisted in the correct identification of the polarity of the membrane.

Patch-Clamp Methodology

Patch pipettes were fabricated from borosilicate glass tubes with an inner filament (ModulOhm, Herlev, Denmark) on a vertical puller (Hans Ochotzki, Homburg, Germany) using a gravity-driven two-step pulling procedure. The pipettes were fire-polished (Micro Forge MF-90; Narishige, Tokyo, Japan) to a final resistance of 5–10 MΩ when filled with NaCl Ringer. An EPC-9 amplifier (HEKA Elektronik, Lambrecht/Pfalz, Germany) furnished with a 50-GΩ headstage was used for voltage clamping and amplification of pipette currents before recording on a digital recorder (DTR-1204; Biologic, Claix, France).

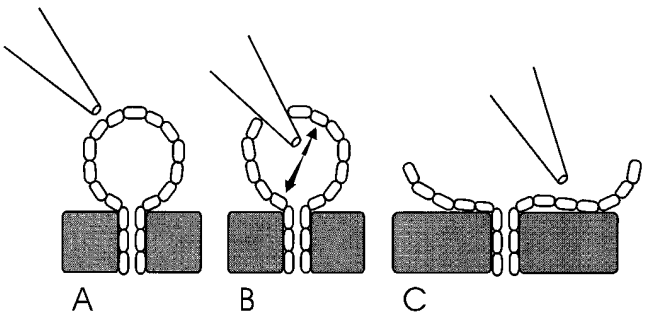

FIGURE 1. Microdissection of frog skin glands from the serosal side. (*A*) The preparation consisted of gland acini stripped for connective tissue and attached to the epithelium via the duct. (*B*) A patch pipette was shoved into the gland lumen and moved to either side to slit open the acinus. (*C*) The two separated acinus halves were pressed against the epithelium, and a new patch pipette was used for forming patches on the apical membrane.

Analysis

For analysis of the channel amplitude, currents were filtered at 100 Hz (in a few cases at 50 Hz) corner-frequency (−3 dB, low pass eight-pole Bessel filter; Frequency Devices Inc., Haverhill, MA) and digitized at 1 kHz sampling frequency through a 1401*plus* interface (Cambridge Electronic Design, Cambridge, UK). Measurement of channel amplitude was performed using Gaussian fits to all-points histograms and the current–voltage relationship constructed accordingly. The current–voltage relationships of Figs. 3, 4, and 6 were fitted using polynomial regression of increasing order, including the highest order that was considered significant ($P < 0.05$) by analysis of variance (ANOVA; Sokal and Rohlf, 1981). The regression procedure was carried out by including all data points from individual experiments and the error associated with the fitted parameters is the standard error of the resulting fit. Since this procedure includes only one fitting event, no error value is associated with derived variables such as the reversal potential.

Determination of the halide selectivity of the channel was done in excised inside-out patches by measuring the reversal potential in symmetrical 120 mM Cl^- and after replacing 100 mM bath Cl^- with either Br^- or I^-. The change in reversal potential upon replacement, ΔV_{rev}, was used for calculation of the permselectivity ratio for the other halide (X) and Cl^-, using the formula

$$\frac{P_X}{P_{Cl}} = \frac{\exp(F \cdot \Delta V_{rev}/RT) \cdot [Cl^-]_o - [Cl^-]_c}{[X]_i}, \quad (1)$$

derived from the Goldman voltage equation. Since the substituted halides and Cl^- have almost identical mobilities, the resulting liquid junction potentials are insignificant (<0.3 mV, calculated following Barry and Lynch, 1991) and have not been corrected for.

For analysis of the single-channel kinetics, currents were filtered at 200 Hz (−3 dB corner frequency, eight-pole Bessel filter) and digitized at 5 kHz. According to double-Lorentzian fits to power density spectra calculated from the same patches (see below), the bandwidth of 200 Hz would include >98% of the band-unlimited variance due to channel gating. The channel open and closed times were determined using a single threshold just below 50% of the full channel amplitude. A minimal time resolution of 1 ms was superimposed on the distribution of open and closed times, and events >4 ms were used for fitting (Colquhoun and Sigworth, 1995).

For stationary noise analysis in multi- or single-channel patches, currents were filtered at a corner frequency of 500 Hz (−3 dB, low pass eight-pole Butterworth; Frequency Devices Inc.) and digitized at 1 kHz. The current was divided into blocks of 4,096 points each (fundamental frequency = 0.244 Hz) and the power density spectrum was estimated using a Fast Fourier Transform. After averaging of the spectra, Lorentzians were fitted using a Levenberg-Marquard routine. In practice, the formula fitted to the spectra was:

$$S(f) = \frac{S_{o1}}{1 + (f/f_{c1})^2} + \frac{S_{o2}}{1 + (f/f_{c2})^2} + S_\infty, \quad (2)$$

where S_{o1}, f_{c1} and S_{o2}, f_{c2} are the low frequency asymptote and corner frequency of the low and high frequent Lorentzian, respectively, and S_∞ is a plateau-level (formally attained as $f \to \infty$) indicating the background noise level in the patch. The (band-unlimited) variance in current ascribable to each Lorentzian was calculated by integration of the Lorentzians at positive frequencies, yielding

$$\sigma_i = \frac{\pi S_{oi} f_{ci}}{2} \quad i \in \{1,2\}. \quad (3)$$

Conventions and Software

In the figures, outward currents (corresponding to an inwardly directed flux of Cl^-) are defined as positive and displayed as upward deflections. Potentials are given as bath referenced to the pipette. Numbers are given as mean ± SEM. Currents used for amplitude and single-channel kinetic analysis were digitized and analyzed using the Patch and Voltage Clamp Software v. 6.24 (Cambridge Electronic Design). For stationary noise analysis, currents were digitized and Fourier transformed using the SPAN-Spectral/Variance analysis program (J. Dempster, University of Strathclyde, Glasgow, UK). Polynomial regression and fitting of multiple Lorentzians (Eq. 2) was performed using Origin 5.0 (Microcal Software Inc., Northampton, MA), which was also used for preparing graphical displays.

Solutions and Chemicals

The standard extracellular NaCl Ringer contained (mM): 113 Na^+, 117.7 Cl^-, 3.7 K^+, 3 acetate, 10 glucose, 5 HEPES, 1 Ca^{2+}, 1 Mg^{2+}, pH 7.4. The standard intracellular solution, denoted I-28, contained (mM): 15 Na^+, 27.9 Cl^-, 105 aspartic acid, 115 Tris, 5 HEPES, 1 EGTA, 1.1 Mg^{2+}, 0.371 Ca^{2+}, pH 7.2, 10^{-7} M free-Ca^{2+}, 10^{-3} M free Mg^{2+}. For measurement of conductance under symmetrical $[Cl^-]$, the intracellular solution denoted "120.6 mM Cl^-" contained (mM) 117.7 Na^+, 120.6 Cl^-, 5 HEPES, 1 EGTA, 1.1 Mg^{2+}, 0.371 Ca^{2+}, pH 7.2, 10^{-7} M free Ca^{2+}, 10^{-3} M free Mg^{2+}. For measurement of halide selectivity, 100 mM Cl^- was replaced by 100 mM Br^- or I^-.

The pipette used for patch clamp contained NaCl Ringer to which in most cases was added 1 mM quinine to block larger K^+ channels of the apical membrane, which otherwise compromised the resolution in cell-attached patches. Quinine inhibits the macroscopic K^+ secretion when the glands are stimulated, whereas Ba^{2+} is ineffective (M.S. Nielsen, personal communication). Cl^- channels obtained with quinine in the pipette did not differ noticeably (e.g., in conductance) from Cl^- channels obtained in the absence of quinine.

Isoproterenol, forskolin, IBMX (isobutyl-1-methyl-xanthine), ATP, DIDS (4,4-diisothiocyanatostilbene-2,2-disulfonic acid), and dibutyryl-cAMP(db-cAMP) were from Sigma Chemical Co. (St. Louis, MO). NPPB (5-nitro-2-(3-phenylpropylamino)benzoic acid) and glibenclamide were from Research Biochemicals, Inc. (Natick, MA). DPC (diphenylamine-2-carboxylic acid) was from FLUKA Chemie (Buchs, Switzerland). cAMP-dependent protein kinase, catalytic subunit, was from Promega (Madison, WI).

DPC was dissolved in 0.1 M NaOH and titrated to pH 7.8 with HCl and H_2SO_4 to a total $[Cl^-]$ of 24 mM and [DPC] of 20 mM. NPPB and glibenclamide were dissolved at 0.1 M in DMSO. DIDS was dissolved in water at a nominal concentration of 10 mM and the dissolution was verified by measurement of the optical density at 342 nm, yielding a concentration of dissolved DIDS of 9.44 mM.

Reference Electrode and Measurements of Liquid Junction Potentials

The reference electrode was connected to bath via an agar bridge made up of NaCl Ringer. When exchanging the solution in the bath for I-28, a well-defined liquid-junction potential appears at the agar bridge, making the potential across the patched membrane, V_M:

$$V_M = -V_p + V_{2,1}, \quad (4)$$

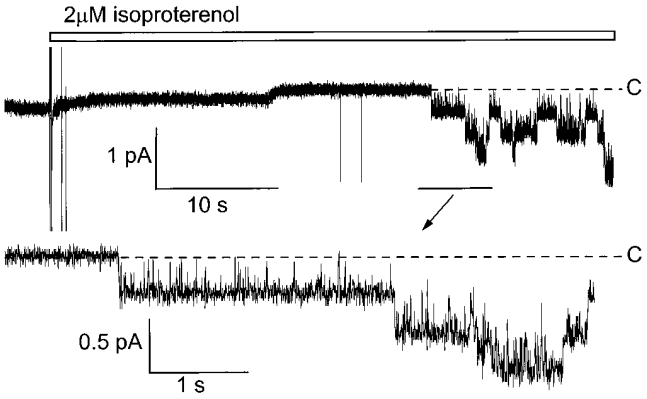

FIGURE 2. Activation of channels by cAMP-inducing substances. Cell-attached patch obtained on the luminal membrane of an unstimulated gland cell and held at $-V_p = -50$ mV. The patch was without channel activity until stimulated by application of 2 μM isoproterenol via the perfusion system (*top*). Activated channels displayed long bursts of activity (*bottom*). C denotes the current level with all channels closed.

where $V_{2,1}$ is the potential of I-28 with respect to NaCl Ringer (Neher, 1992). This potential was measured against a free-flowing 2 M KCl electrode according to Neher (1992), yielding $V_{2,1} = -3.71 \pm 0.05$ mV ($n = 6$). All accepted measurements were reversible within 0.11 mV.

RESULTS

Cell-attached Patches

Activation of channels. In cell-attached patches obtained on unstimulated (resting) gland cells, the application of 2 μM isoproterenol induced activity by small Cl^--selective channels in ~60% of the cases (20 of 34 patches) (Fig. 2). Similar channels were induced by application of 12.5 μM forskolin (14 of 31 patches) or by 0.5 mM db-cAMP and 0.1 mM IBMX (12 of 22 patches). Fig. 2 shows the characteristic long bursts of activity upon stimulation. The time-delay before the first burst of activity lasting at least 1 s was significantly shorter with isoproterenol (56 ± 7 s, $n = 20$, the "dead time" in the perfusion system was 20–30 s and is included in the time-delay) than with either forskolin (105 ± 12 s, $n = 14$; $P < 0.001$, Mann-Whitney U test) or db-cAMP and IBMX (110 ± 13 s, $n = 12$, $P < 0.005$, Mann-Whitney U test).

Current–voltage relationship. Fig. 3 shows the average current–voltage relationship (*A*) of cells stimulated with cAMP-inducing agents and an example of channel gating (*B*) at different holding potentials. Note the long bursts of activity and the increased number of brief closings ("gaps") at hyperpolarized potentials, which were seen consistently in cell-attached patches. The current–voltage relationship saturated at negative potentials (Fig. 3 *A*), and a cubic polynomium was required for an accurate description (ANOVA: linear and

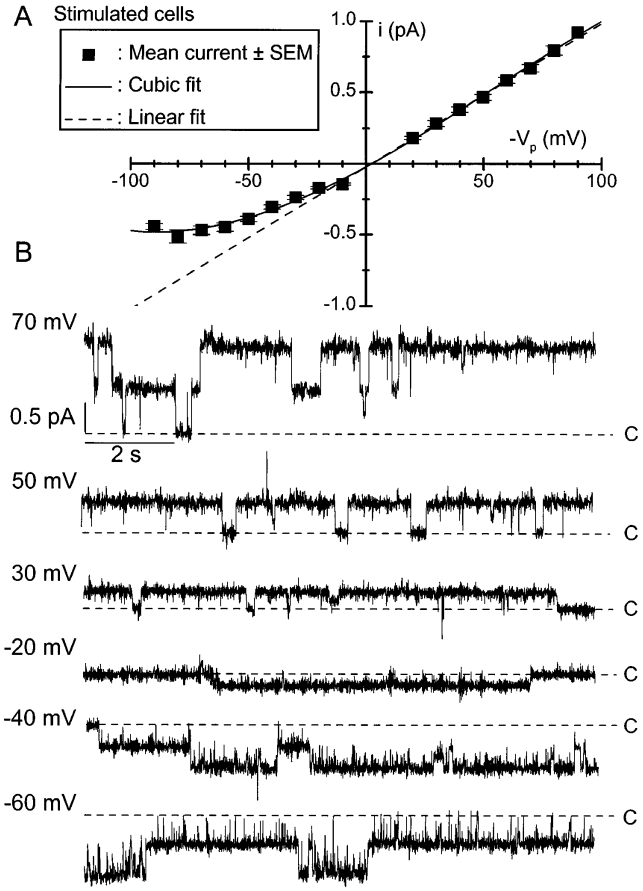

FIGURE 3. (*A*) Mean current–voltage relationship for nine cell-attached patches stimulated by cAMP-inducing substances. Symbols show mean current ± SEM for one to nine determinations at each potential. The current–voltage relationship was fitted with cubic regression. Points at positive potentials were fitted with linear regression as well. (*B*) Example of channels gating at different potentials ($-V_p$) in the cell-attached configuration. Note faster gating at negative potentials.

quadratic regression, $P < 0.001$; cubic regression, $P < 0.005$; quintic regression, $P > 0.10$; 110 data points from nine experiments). When considering only positive potentials, the current–voltage relationships showed no significant deviations from linearity (ANOVA: linear regression, $P < 0.001$; quadratic regression, $P > 0.50$; 51 data points from nine experiments) and had a conductance of 10.0 ± 0.4 pS. The estimated reversal potential was 1.2 mV (i.e., close to 0 mV), indicating that $V_c \approx E_{Cl}$ (since $V_{rev} = E_{Cl} - V_c$). Thus, Cl^- is apparently in equilibrium after activation by cAMP (see DISCUSSION).

In cell-attached patches on unstimulated (resting) gland cells, spontaneous Cl^- channel activity was also noted occasionally. In most cases, the reversal potential was >0 mV (range: −0.22 to 55.4 mV, mean ± SEM = 28.1 ± 6.7 mV, $n = 9$), indicating that intracellular Cl^- was above electrochemical equilibrium at the spontane-

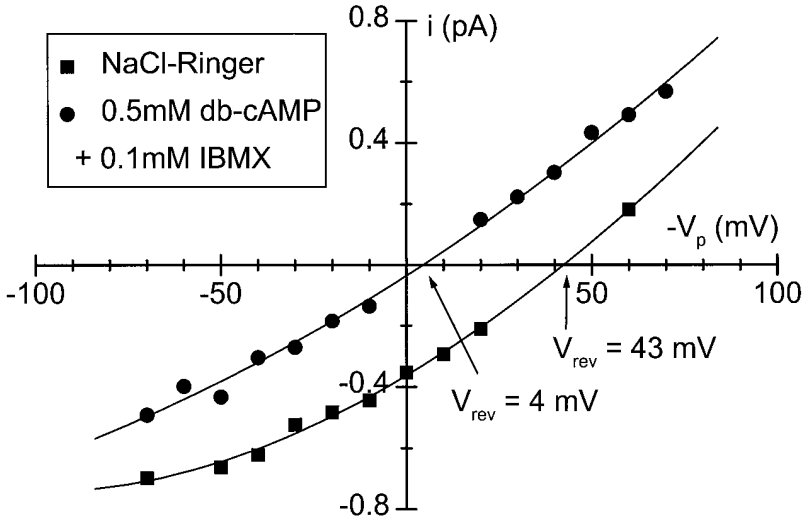

FIGURE 4. Current–voltage relationship for a small Cl^- channel in a cell-attached patch before (■) and during (●) stimulation with db-cAMP and IBMX. Reversal potentials, V_{rev}, were 43 mV before and 4 mV during stimulation.

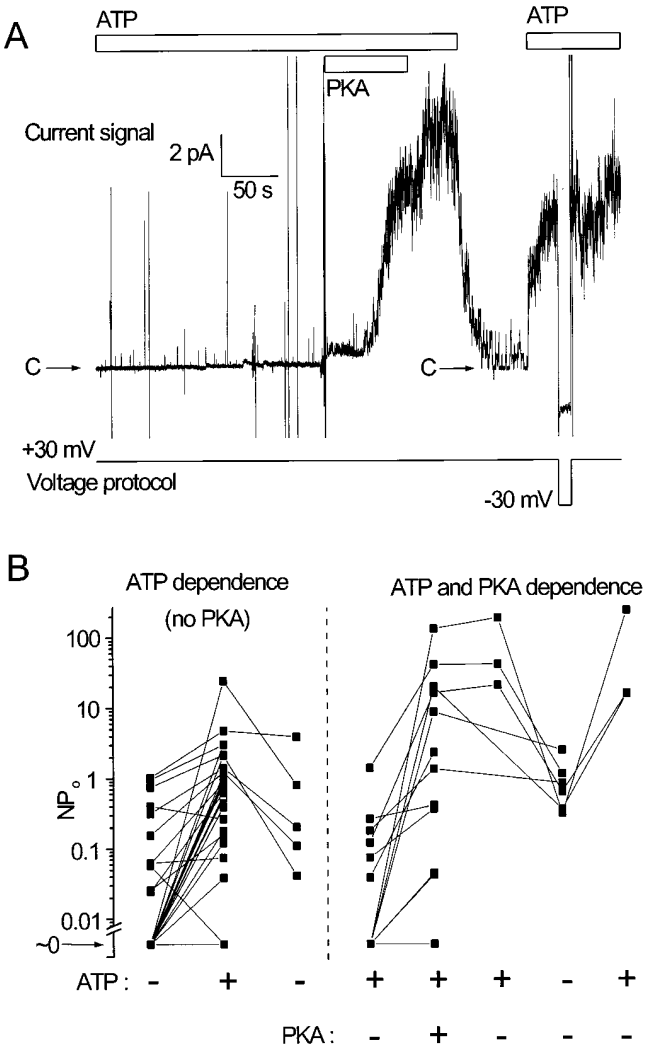

FIGURE 5. Regulation by protein kinase A and ATP. (*A*) Compressed view (note scale bar) of the current in an inside-out patch held at $-V_p$ = 30 mV and perfused with I-28 on the cytoplasmic side. Bars indicate addition of 1.5 mM ATP and 65 nM protein kinase A catalytic subunit. Perfusion was stopped during addition of PKA directly to the bath. Both mean current and current noise increased upon addition of PKA, indicating increased channel gating from multiple channels. Clamping the voltage transiently to −30 mV, close to the equilibrium potential for Cl^-, reduced the current noise to control values, indicating Cl^- selectivity of the activated channels. Single-channel gating could only be clearly distinguished during wash without ATP. (*B*) Quantification of the effect of ATP and PKA on inside-out patches. NP_o (note logarithmic axis) was measured as explained in the text. To the left is shown the effect of ATP (1.5 mM) addition and removal to patches freshly excised from the cell. To the right is shown effect of PKA addition and subsequent ATP removal/readdition to inside-out patches.

ous membrane potential, V_c. The reversal potential of the channel in Fig. 4 changed 39 mV to the left upon stimulation by db-cAMP and IBMX. Assuming a constant $[Cl^-]_c$, this could be taken as evidence for a 39-mV depolarization of V_c after stimulation by cAMP.

Inside-Out Patches

Regulation of channels. In most cases, channel activity was lost upon patch excision into intracellular solution (I-28) devoid of ATP. In 31 of 68 patches (patches with and without activity in cell-attached configuration are included), channel activity was noted during exposure of the cytosolic side of the membrane to 1.5 mM ATP. Channel activity was quantified in terms of NP_o (N = number of channels, P_o = open probability) by measuring mean macroscopic current $\bar{I}$ (leakage current subtracted), and dividing by the mean current through one channel, $\bar{i}$ (see Fig. 6, below) measured at the same potential. The resulting activity measurements show that channel activity was dependent on ATP after excision to the inside-out configuration (Fig. 5 *B, left*). Channel activity increased further in 11 of 16 cases (only counting patches where unambiguous channel activity was observed after excision) when the patch was

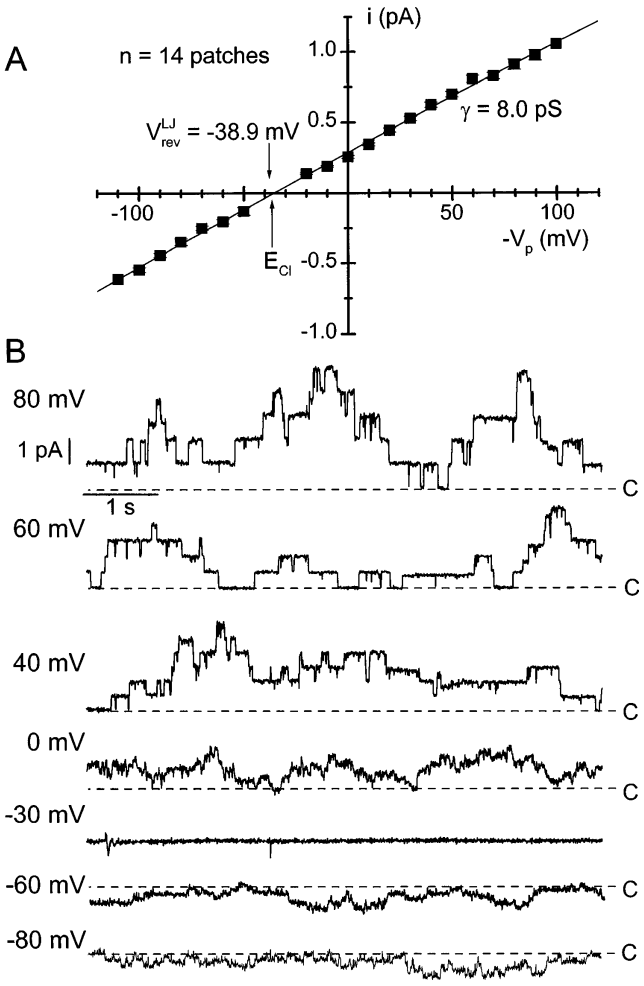

FIGURE 6. (*A*) Mean current–voltage relationship for inside-out patches bathed with I-28 on the inside. Symbols show mean current ± SEM for 1–14 determinations at each potential. Conductance and reversal-potential (corrected for liquid junction potential, $V_{rev}^{LJ} = V_{rev} + V_{LJ}$) calculated from linear regression analysis are indicated. (*B*) Example of channels gating at different potentials ($-V_p$) in the inside-out configuration. No gating was seen at −30 mV, close to E_{Cl}.

exposed to the catalytic subunit of cAMP-dependent protein kinase (16–66 nM, corresponding to 50–200 casein U/ml) (Fig. 5, *A* and *B*). After phosphorylation, the channels were active even in the absence of protein kinase, as long as ATP was present at the inside of the membrane. Removal of ATP, however, caused a reversible loss of activity (Fig. 5, *A* and *B*). This mode of regulation is identical to the dual phosphorylation/ATP dependence of the CFTR Cl^- channel (Tabcharani et al., 1991; Anderson et al., 1991). No rundown of channel activity was noted in the presence of ATP even after removing cAMP-dependent protein kinase. Thus endogenous protein phosphatase activity was apparently not present in excised patches.

Current–voltage relationship. When bathed with intracellular solution and ATP, the channel reversed close to the calculated reversal potential for Cl^- (Fig. 6). In spite of the skewed Cl^- concentrations in this case, the current–voltage relationship showed no significant deviations from linearity (ANOVA: linear regression, $P < 0.001$; quadratic regression, $P > 0.75$; 158 data points from 14 experiments). Linear regression yielded a conductance of 8.0 ± 0.1 pS and a reversal potential at −38.9 mV when corrected for liquid junction potential (Eq. 4). Since the equilibrium potential for Cl^- was −36.4 mV, no aspartate permeability was detected.

Substates. The channels displayed a characteristic substate (Fig. 7 *A*) in most patches. The amplitude of this substate was measured using Gaussian fits to all-points histograms (Fig. 7 *B*) and expressed as a fraction of the full amplitude. This measurement was feasible at positive holding potentials only, where amplitudes were high and activity levels stationary over a long period of time. The distribution of relative substate amplitudes from 25 patches showed a variable substate level, from 0.37 to 0.67, with predominance around or just below 2/3 of the full amplitude (Fig. 7 *C*). Thus, the substates did not reveal any obvious oligomeric organization of the channel, in which case the substates would be expected to assemble around levels that would constitute multiples of an integer fraction of the full amplitude (e.g., if three parallel pores were to form the functional channel, two peaks in the substate histogram would a priori be expected, at 1/3 and 2/3 of the full amplitude).

Halide selectivity. In inside-out patches bathed in 120.6 mM Cl^- (MATERIALS AND METHODS), the channels (shown to be Cl^- selective by a control period in I-28) displayed a linear current–voltage relationship with a conductance of 10.3 ± 0.3 pS (five experiments). When 100 mM Br^- substituted for Cl^- in the bath, the current–voltage relationship was still linear, when considering either positive or negative potentials, however, the slopes were different (Fig. 8). To be able to estimate conductance at positive and negative potentials (denoted γ^+ and γ^-, respectively) together with the reversal potential, V_{rev}, the following equations were fitted to the data:

$$i_{channel} = \gamma^+ \cdot (-V_p - V_{rev}) \quad \text{for } -V_p > 0 \text{ mV}$$
$$i_{channel} = \gamma^- \cdot (-V_p - V_{rev}) \quad \text{for } -V_p < 0 \text{ mV}. \qquad (5)$$

The two fits (positive and negative potentials) were carried out simultaneously, minimizing the total sum of squares between data points and model, so that all points were applied for estimating V_{rev}. The results showed that the conductance at negative potentials (when Br^- was permeating the channel) was markedly depressed (5.4 ± 0.3 pS, $n = 5$) with respect to the conductance at positive potentials (10.2 ± 0.6 pS, $n = 5$) or

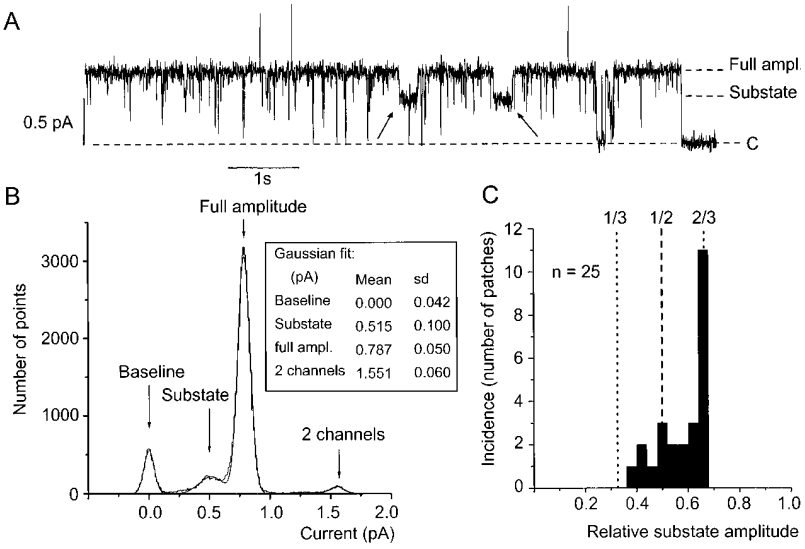

FIGURE 7. Substates. (*A*) Current trace of inside-out patch held at 60 mV. Substates of the small Cl^- channel shown by arrows. (*B*) Histogram of the patch shown in *A* (longer trace included in the histogram) illustrates the determination of substate amplitude. Superimposed are Gaussian distributions (mean and SD shown in the box) used for determination of current amplitudes associated with each level. The fractional amplitude of the substate was calculated as 65% of the full amplitude. (*C*) Distribution of fractional substate amplitudes in 25 patches.

when only Cl^- was present. In spite of the reduced conductance when the current was carried by Br^-, the reversal potential shifted 14.3 mV to the right (i.e., away from E_{Cl}, Fig. 8), indicating a larger permeability to Br^-. Applying Eq. 1 yielded a permeability ratio between Br^- and Cl^- of 1.90.

When 100 mM I^- replaced Cl^- in the bath, the conductance at positive potentials was 6.0 ± 0.6 pS (n = 3) and no current could be detected in the inward direction; i.e., the conductance for I^- was not detectable. Regardless, the extrapolated reversal potential shifted 5.7 mV to the right, yielding a formal permeability for I^- at 1.3× that of Cl^-.

Pharmacology. Inside-out patches with stationary channel activity when exposed to I-28 and 1.5 mM ATP on the inside were used for investigating the pharmacology of the channel. Putative blockers were added to I-28 in the presence of ATP and applied via the perfusion system. Treatment of the channels with 100 μM NPPB caused a decrease in current in single- or multichannel patches (seven of seven patches investigated), apparently caused by brief interruptions of the open state (Fig. 9). The block was relieved when the patch was perfused with control solution (I-28 and 1.5 mM ATP). Treatment with glibenclamide (100–200 μM, effective in nine of nine patches) or DPC (1 mM, effective in six of six patches) likewise induced a partial and fully reversible block characterized by increased flickering (Fig. 9). Especially in the case of DPC, it appeared that the amplitude of the channel was also depressed, but this could be caused by high frequency flickering beyond the bandwidth investigated (100 Hz in Fig. 9). Indeed, McCarty et al. (1993) reported that DPC block of CFTR results in interruptions of the open state with a time constant <1 ms, which would not have been resolved by our experiments.

Treatment with 200–300 μM DIDS caused within seconds a complete and irreversible block of channel cur-

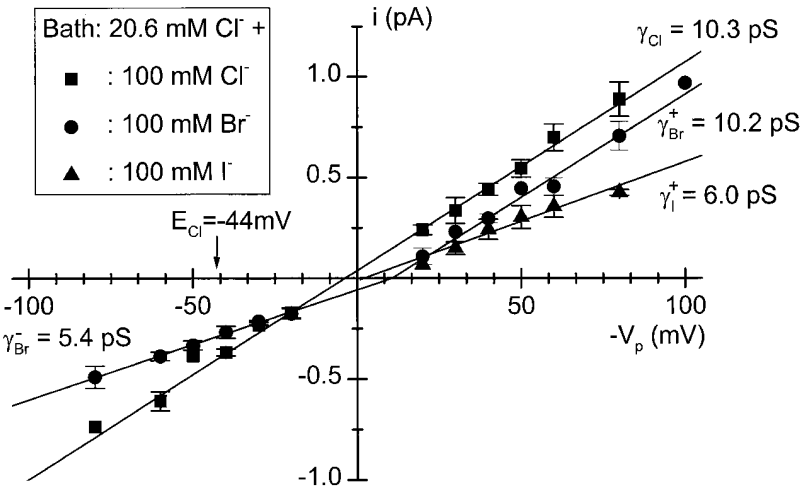

FIGURE 8. Current–voltage relationship (mean ± SEM) for inside-out patches exposed to 120.6 mM Cl^- (■), or 20.6 mM Cl^- and 100 mM Br^- (●) or 100 mM I^- (▲) on the inside. The current–voltage relationships for 120.6 mM Cl^- and 100 mM I^- were fitted with a straight line, whereas the relationship for 100 mM Br^- was fitted with Eq. 5 (see text). Conductances are indicated.

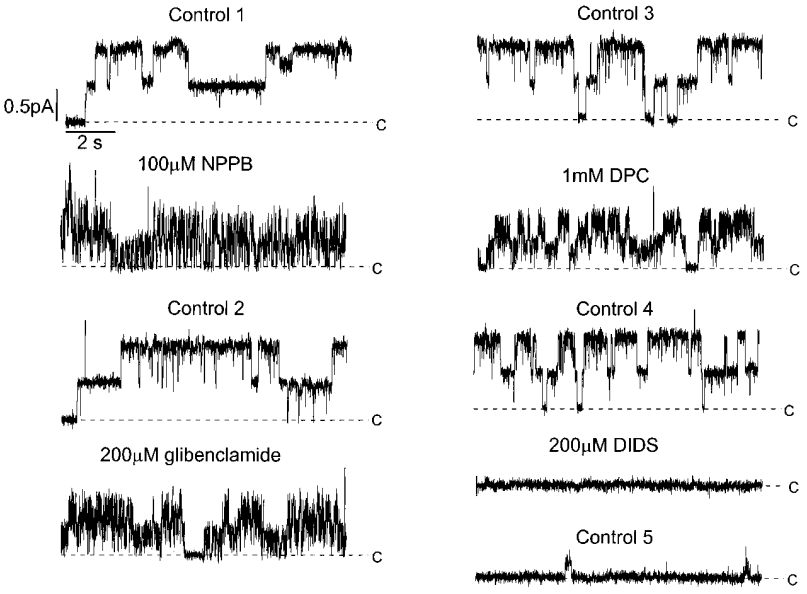

FIGURE 9. Pharmacology. Inside-out patch with two active Cl^- channels held at $-V_p = 50$ mV. In "Control" periods 1–5, the patch was washed with I-28 + 1.5 mM ATP on the inside. Sequential addition of putative blockers to I-28 + 1.5 mM ATP are indicated. In Control period 5, the patch was washed for 6 min without DIDS. Note the appearance of channel transitions with depressed amplitude.

rent in both single- and multichannel patches (five of six patches investigated[2]). Even when washing the patch for 15 min with 30 ml of control solution (corresponding to ~60× bath volume), channel activity did not recover. However, after a while, small channel-like transitions of depressed amplitude were often noted (Fig. 9).

Single-channel kinetics. The kinetics of the channel was likewise investigated in inside-out patches exposed to I-28 and ATP and held at positive voltages. This yielded the most stationary channel activity, and the best signal to noise ratio. Two patches where only a single channel was observed were found to be of sufficient quality to allow analysis. The open time distribution was in both cases characterized by a single peak in a logarithmically binned histogram (Fig. 10 *B*), which could be satisfactorily fitted with a single exponential component, indicating a mean open time of 85.6 ms (Fig. 10 *B*) or 230 ms (data from the other patch, not shown). The closed time distribution exhibited two peaks and was fitted using a double exponential model. The fast time constant was 16.4 ms (7.6 ms in the other patch)

[2]The nonresponsive patch also did not respond to removal of ATP with a decreased channel activity; thus, apparently, the channels or the patch configuration were unusual.

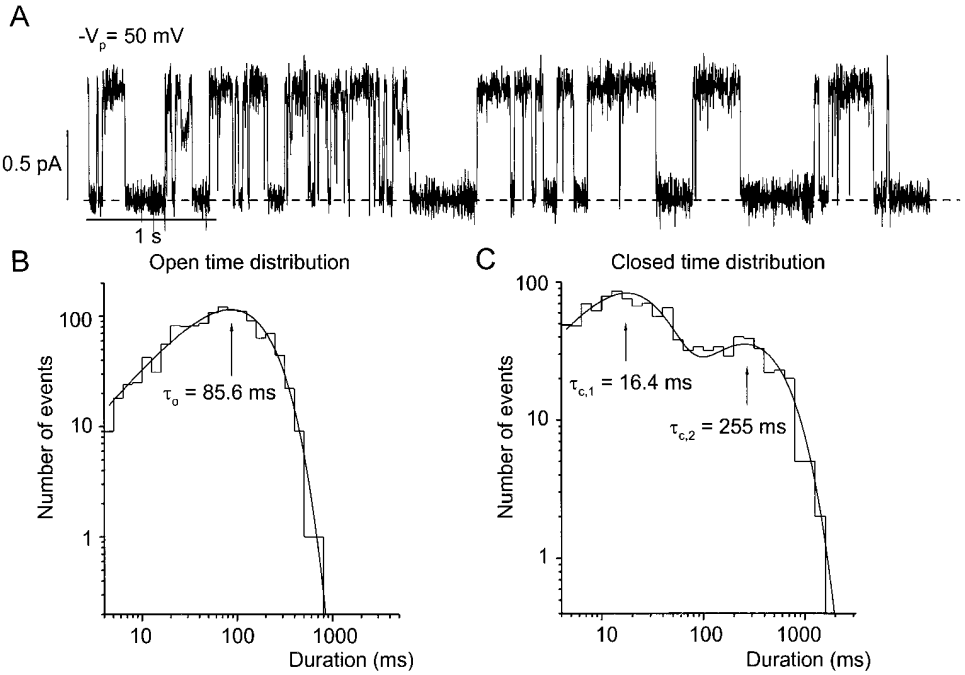

FIGURE 10. Single-channel kinetics. (*A*) Current trace showing activity of a single channel at $-V_p = 50$ mV filtered at 200 Hz. (*B*) Open time distribution displayed using logarithmic binning and logarithmic ordinate axis. Fitted exponential superimposed. (*C*) Closed time distribution displayed using logarithmic binning and logarithmic ordinate axis. Fitted sum of two exponentials superimposed. Exponentials were fitted using the maximum likelihood method.

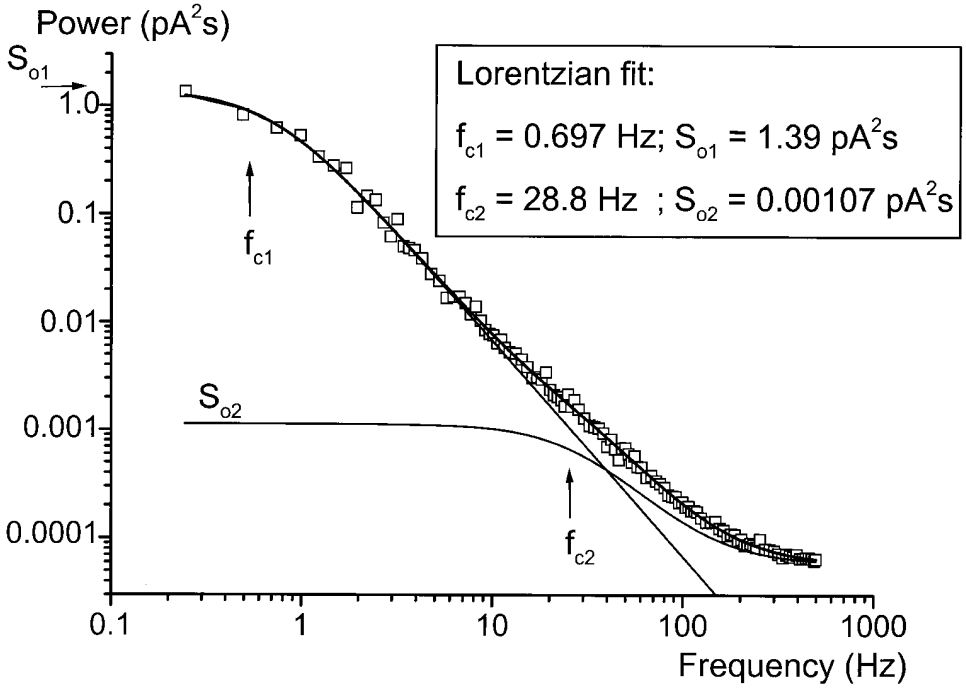

FIGURE 11. Power density spectrum calculated from multichannel inside-out patch held at $-V_p$ = 30 mV in the presence of ATP (in I-28) on the inside. Symbols show measured spectrum, top line indicates the fitted sum of two Lorentzian plus a plateau-level (Eq. 2) with the parameters shown in the box. Separate lines show the higher and lower frequency Lorentzian, respectively.

and the slow one was 255 ms (193 ms in the other patch). Thus, a minimum kinetic model of the channel would comprise one open and two closed states.

Analysis of stationary current fluctuations. In single- or multichannel patches, the kinetic analysis was extended by calculating the one-sided power density spectrum (PDS) using Fast Fourier Transformation of the current traces. In each case, the PDS was initially fitted with a single Lorentzian and a plateau-level and the fit compared with the PDS data points. In 12 of 14 patches, a second Lorentzian was required to obtain a reasonable fit. When fitting the second Lorentzian (Eq. 2), the parameters of the first (low frequency) Lorentzian were fixed and only the second Lorentzian and the plateau-level, S_∞, were allowed to vary. The fit of two Lorentzians described the PDS well in the 12 remaining patches (Fig. 11). The fitted corner frequencies in double-Lorentzian patches were 0.85 ± 0.11 Hz (n = 12) and 27.9 ± 2.9 Hz (n = 12) for the low and high(er) frequency Lorentzian, respectively. Calculation of the band-unlimited current variance contributed by each Lorentzian by Eq. 3 revealed a ratio of slow to fast component variance (σ_s/σ_f) of 16.1 ± 4.7 (n = 12), thus the low frequency Lorentzian contributed most of the noise.

DISCUSSION

Function of Luminal Cl^- Channels in Secretion

According to the current model (e.g., Petersen, 1992; Greger, 1996), Cl^- secretion is accomplished by the serial arrangement of a luminal conductance together with a driving force for Cl^- and a basal conductance and driving force for K^+. Activation of the luminal Cl^- conductance drives Cl^- out in the lumen. Due to the electrical shielding of the lumen by the resistance of the paracellular pathway to anion flow, this will cause a lumen-negative potential, which will cause Na^+ to follow paracellularly. In the frog skin glands, the mucosal potential drops close to zero after 30–60 min of stimulation, and it was recently suggested that in this state of the gland, Na^+ secretion is active, not passive (Ussing et al., 1996). However, in both models, the serial arrangement of batteries favoring Cl^- and K^+ efflux is assumed.

In the present study, we have succeeded in identifying an apically located conductance for Cl^-, consisting of small 8-pS channels in the luminal membrane. These channels were demonstrated to be activated by the cAMP cascade on the following levels: activation of β-adrenergic receptors using isoproterenol, activation of the adenylate cyclase using forskolin, direct elevation of cellular [cAMP] using a membrane-permeable cAMP analogue together with the phosphodiesterase inhibitor IBMX, and finally activation of channels in excised inside-out patches by exposure to the catalytic subunit of cAMP-dependent protein kinase. We conclude that in the frog skin gland a CFTR-like channel-type mediates cAMP-dependent Cl^- secretion.

It should be noted that we did not encounter any other type of Cl^- channel in the luminal membrane on a regular basis. Only in two to three patches obtained in the beginning of the study was a very large Cl^- channel (conductance 150–200 pS) seen. The identity, regu-

lation, and function of this channel are unknown. Thus, it would appear from the current data that a single population of Cl^- channels is present in the apical membrane to serve the function of Cl^- secretion. This is an important finding in view of the different types of cells found in the mucous/seromucous glands of frog skin: a (mucous/seromucous) cell type with secretory granules, a cell type without granules but with pronounced amplification of the basolateral membrane, and a mitochondria-rich cell type (Mills and Prum, 1984). Either these cells have identical Cl^- channels in the apical membrane or, for whatever reason, we have only been patching one type of cells. Furthermore, ~50% of cell-attached patches did not activate when stimulated with cAMP-inducing agents, thus it is possible that at least one cell-type could be devoid of cAMP-stimulated Cl^- channels in the luminal membrane. Engelhardt et al. (1994) reported that CFTR message and protein was predominantly expressed in the mucous cell type in *Xenopus* glands.

To achieve sustained secretion, active K^+ channels are assumed in the secretory model, the function of which are to recycle K^+ that enters the cell through the basolateral Na/K/2Cl cotransporter and the Na/K-ATPase and further to provide a driving force for Cl^- by upholding the inequality $V_c < E_{Cl}$. In cell-attached patches, this inequality would correspond to a reversal potential for Cl^- channels at positive potentials. Data from unstimulated cells showed that the inequality was satisfied in the resting state of the gland. In stimulated cells, however, Cl^- channels reversed at 0 mV applied potential, meaning that $V_c \approx E_{Cl}$ after activation by cAMP-inducing substances. The same result was obtained in whole-cell patches (Sørensen and Larsen, 1997). Thus, there is no apparent driving force for Cl^- exit after stimulation, meaning that K^+ channels were not substantially activated. An alternative is that the driving force is so low, probably <4 mV, that we cannot find it in our studies. In a study of basolateral K^+ channels in the same kind of preparation, Andersen et al. (1995) found a "maxi" K^+ channel of unitary conductance ~200 pS. However, this K^+ channel had very low basal open probability (0.018 ± 0.005), and a rise in cytosolic Ca^{2+} by muscarinic stimulation was required to achieve activation. Therefore, in this gland type it would appear that after stimulation by cAMP-inducing substances the magnitude of the K^+ conductance is limiting net secretion. This contrasts to the situation in shark rectal gland, where cAMP-dependent stimulation causes depolarization to −63 mV (apical membrane potential) where E_{Cl} = −48 mV (calculated from Greger et al., 1984) and where Cl^- channel currents in activated cells reversed at +25 mV applied potential (Greger et al., 1987). Likewise, in colon crypts, the stimulation by cAMP causes a primary depolarization and a secondary hyperpolarization caused by activation of cAMP-dependent K^+ channels (Lohrmann and Greger, 1993). However, Becq et al. (1993*b*), using primary cultures of human tracheal gland cells, obtained results similar to ours, that small cAMP-activated Cl^- channels reversed at 0-mV applied potential.

In the whole frog skin preparation, the glands can be stimulated to stationary secretion by isoproterenol (Thompson and Mills, 1983) or prostaglandin E_2 (Bjerregaard and Nielsen, 1987), which apparently acts exclusively on the cAMP pathway. This would seem to require activation of K^+ channels. Thus, we cannot rule out the possibility that the collagenase treatment and/or isolation of the glands from the connective tissue have impaired a K^+ conductance in the basolateral membrane.

Identity of the Small Luminal Chloride Channel

The small unitary conductance (8.3 pS), together with the dependence of the channel on cAMP in cell-attached patches and of protein kinase A–dependent phosphorylation in inside-out patches and the obligatory requirement for ATP in the phosphorylated state, constitute the functional distinguishing properties for the CFTR-encoded Cl^- channel (Tabcharani et al., 1991; Anderson et al., 1991). As previously noted, the CFTR message and protein have been localized to the submucosal glands in *Xenopus* (Engelhardt et al., 1994), and the conclusion that the apical Cl^- channel in the frog skin glands is CFTR is, therefore, in our view unescapable.

Rectification and Conductance

Single-channel CFTR currents obtained in cell-attached patches have been reported to rectify slightly in the outward direction (Haws et al., 1992; Gray et al., 1989; Tabcharani et al., 1991), which was originally ascribed to the different Cl^- concentrations present on the two sides of the membrane. In the frog skin gland, Cl^- currents saturated at negative potentials, giving the current–voltage relationship an outwardly rectifying appearance. When we fitted the Goldman-Hodgkin-Katz (GHK) current equation to the data by allowing the intracellular Cl^- concentration and membrane potential to vary, the values obtained (fitted parameters were: $[Cl^-]_c$ = 46.4 ± 6.3 mM, V_c = −26.8 ± 4.2 mV, P_{Cl} = 3.3[±0.3] [10^{-14} cm^3 s^{-1}]) agree well with values obtained by other methods ($[Cl^-]_c$ = 38.5 mM (mucous cells), 43.6 mM (gland cells, electron microprobe technique, Mills et al., 1985) and V_c = −28.4 mV (whole-cell patches, Sørensen and Larsen, 1997). Nevertheless, we are able to conclude that the rectification seen in cell-attached patches cannot result from Goldman rectification based on the following observations. (*a*) The

current–voltage relationship when considering only positive currents did not rectify but could be fitted with linear regression. This is not predicted by the GHK equation. (*b*) When fitting the current–voltage relationship in the inside-out configuration under conditions of symmetrical Cl^- concentrations (Fig. 8) with the Goldman-Hodgkin-Katz current equation, the resulting estimated single-channel permeabilities was 2.2×10^{-14} $cm^3\,s^{-1}$. Thus, the channel has much lower permeability in the inside-out configuration, compared with that predicted from cell-attached measurements ($3.3[\pm 0.3] \times 10^{-14}$ $cm^3\,s^{-1}$). (*c*) In inside-out patches exposed to a larger Cl^- concentration gradient (inside: 25 mM, outside: 118 mM) than experienced in cell-attached patches (inside: ~40 mM, outside: 118 mM), the current–voltage relationship was linear.

By the use of dialyzed whole-cell patches (Overholt et al., 1993, 1995) or excised inside-out patches (Linsdell and Hanrahan, 1996*a*; Linsdell et al., 1997) it has been demonstrated that CFTR currents under a range of conditions do not obey the GHK equation, but that excess outward rectification results from a voltage-dependent block by the anions (gluconate, glutamate) usually substituted for Cl^- in making up intracellular-like solutions. It was suggested that during cell-attached recordings outward rectification could result from both the Cl^- concentration gradient and from block by large intracellular anions (Overholt et al., 1993; Linsdell and Hanrahan, 1996*a*). In our case, we fail to find any evidence of GHK behavior. Instead, we suggest that rectification in cell-attached patches is due solely to a voltage-dependent block. This block can apparently not be mimicked by aspartate, which was used at the inside of inside-out patches in the present study.

The conductance of the frog CFTR channels was found to be 10.0 pS for outgoing currents obtained in cell-attached patches, 8.0 pS when bathed with 28 mM Cl^- on the inside, and 10.4 pS in symmetrical 125 mM Cl^-. These are higher than the typical values reported for mammalian CFTR (4–8 pS, Gray et al., 1990; Larsen et al., 1996; Price et al., 1996; Linsdell and Hanrahan, 1996*a*; Tabcharani et al., 1997), but agrees with measurements on *Xenopus* CFTR under conditions of high cytosolic Cl^- (9.6 pS, Price et al., 1996).

Halide Selectivity

Experiments on halide selectivity showed that even though $P_{Br}/P_{Cl} > 1$, the conductance when Br^- is permeating the channel is only half of that when the permeating anion is Cl^-. Tabcharani et al. (1997) using human CFTR expressed in CHO cells obtained the same result. Qualitatively similar results were obtained by I^- substitution, but in this case the conductance for I^- was not measurable. These data are in agreement with previously reported results obtained by cytosolic I^- substitution in human CFTR (Tabcharani et al., 1992). However, more recently it was reported that two states exist in the human CFTR Cl^- channel: one (I_{unbl}) that has simultaneously $P_I/P_{Cl} > 1$ and $G_I/G_{Cl} > 1$, and another (I_{bl}) that has $P_I/P_{Cl} << 1$ and $G_I/G_{Cl} < 1$ (Tabcharani et al., 1997). This is not in agreement with our data, which shows $P_I/P_{Cl} > 1$ and $G_I/G_{Cl} << 1$. However, for *Xenopus* CFTR, Price et al. (1996) showed that in the whole-cell situation the permeability for I^- is higher than for Cl^-, whereas the conductance is less; this was ascribed to a difference in amino acid sequence in the first and second membrane-spanning domain between human and *Xenopus* CFTR.

The results on conductance, rectification, and halide selectivity when taken together are consistent with the idea that two or more anion binding sites are present at the cytosolic side of the channel (Linsdell et al., 1997). Binding of anions other than Cl^- to these sites may cause rectification as seen in cell-attached patches and when substituting Br^- for Cl^-. The intracellular Cl^- concentration may in turn affect the conductance even for outgoing currents; i.e., for an inwardly directed Cl^- flux. Thus, a lower conductance for Cl^- was observed in inside-out patches exposed to 25 mM Cl^- on the inside (Fig. 6) than in cell-attached patches (measured intracellular Cl^- concentration: 38–44 mM, Mills et al., 1985) or when exposed to 120 mM Cl^- on the inside (Fig. 8). Finally, a higher affinity at the first binding site for a weakly permeant ion (Br^-, I^-) may cause the reversal potential to shift in favor of that ion, even when the ion is not or barely able to carry any current through the pore itself.

Pharmacology

The pharmacology of CFTR is usually described as block by one or more of the compounds NPPB, DPC, or glibenclamide, and insensitivity to DIDS. In the present investigation, we found that NPPB, DPC, and glibenclamide added to the cytoplasmic face of inside-out patches caused a partial block characterized by increased flickering, suggesting an interaction with the open channel. This is consistent with investigations on the exact mode of interaction of these blockers with CFTR (DPC: McCarty et al., 1993; glibenclamide: Schultz et al., 1996; Sheppard and Robinson, 1997). However, we also found that DIDS caused an irreversible block of the channels when added to the cytosolic side of inside-out patches. This was an unexpected finding, since DIDS sensitivity is usually ascribed to the outwardly rectifying chloride channel (Bridges et al., 1989) and, indeed, DIDS insensitivity is widely used as a distinquishing property of CFTR in whole epithelia (Shen et al., 1995), in whole-cell patches (Schwiebert et al., 1994),

and when making single-channel measurements (Jovov et al., 1995). In most cases, DIDS has been added to the extracellular side of the membrane (e.g., Gray et al., 1990; Schwiebert et al., 1994; Shen et al., 1995; Larsen et al., 1996). Some investigators, however, have used a protocol similar to ours (i.e., adding DIDS to the cytoplasmic side of inside-out patches or to both sides of reconstituted CFTR) and they failed to see any effect (Egan et al., 1992; Becq et al., 1993*a*; Jovov et al., 1995). We have obtained evidence from the frog skin gland that DIDS is ineffective at concentrations up to 500 μM when added to the outside of outside-out patches (data not shown). Linsdell and Hanrahan (1996*b*) reported that, when added to the inside, DIDS was able to block macroscopic CFTR currents recorded from excised patches of stably transfected Chinese hamster ovary cells. Even though they did not comment on reversibility, the block described by Linsdell and Hanrahan (1996*b*) was voltage dependent and would therefore probably involve a reversible interaction with the channel pore. Further, they state that DIDS caused brief interruptions of the channel's open state, again indicating reversibility. In the present study, the block was irreversible and, within seconds, the currents were blocked completely, even in multi-channel patches with many active channels. Thus, apparently, this is a phenomenon distinctive from that described by Linsdell and Hanrahan (1996*b*) and more resembling the block of the outwardly rectifying Cl^- channel (Bridges et al., 1989).

This study was supported by the Danish Natural Science Research Council (grant 11-0971) and the Carlsberg Foundation.

Original version received 29 December 1997 and accepted version received 26 March 1998.

REFERENCES

Andersen, H.K., V. Urbach, E.V. Kerkhove, E. Prosser, and B.J. Harvey. 1995. Maxi K^+ channels in the basolateral membrane of the exocrine frog skin gland regulated by intracellular calcium and pH. *Pflügers Arch.* 431:52–65.

Anderson, M.P., H.A. Berger, D.P. Rich, R.J. Gregory, A.E. Smith, and M.J. Welsh. 1991. Nucleoside triphosphates are required to open the CFTR chloride channel. *Cell.* 67:775–784.

Barry, P.H., and J.W. Lynch. 1991. Liquid junction potentials and small cell effects in patch-clamp analysis. *J. Membr. Biol.* 121:101–117.

Becq, F., E. Hollande, and M. Gola. 1993*a*. Phosphorylation-regulated low-conductance Cl^- channels in a human pancreatic duct cell line. *Pflügers Arch.* 425:1–8.

Becq, F., M.D. Merten, M.A. Voelckel, M. Gola, and C. Figarella. 1993*b*. Characterization of cAMP dependent CFTR-chloride channels in human tracheal gland cells. *FEBS Lett.* 321:73–78.

Bjerregaard, H.F., and R. Nielsen. 1987. Prostaglandin E2-stimulated glandular ion and water secretion in isolated frog skin (*Rana esculenta*). *J. Membr. Biol.* 97:9–19.

Bridges, R.J., R.T. Worrell, R.A. Frizzel, and D.J. Benos. 1989. Stilbene disulfonate blockade of colonic secretory Cl^- channels in planar lipid bilayers. *Am. J. Physiol.* 256:C902–C912.

Colquhoun, D., and F.J. Sigworth. 1995. Fitting and statistical analysis of single-channel records. *In* Single-Channel Recording. B. Sakman and E. Neher, editors. 2nd edition. Plenum Publishing Corp. New York. 522–524.

Egan, M., T. Flotte, S. Afione, R. Solow, P.L. Zeitlin, B.J. Carter, and W.B. Guggino. 1992. Defective regulation of outwardly rectifying Cl^- channels by protein kinase A corrected by insertion of CFTR. *Nature.* 358:581–584.

Engelhardt, J.F., S.S. Smith, E. Allen, J.R. Yankaskas, D.C. Dawson, and J.M. Wilson. 1994. Coupled secretion of chloride and mucus in skin of *Xenopus laevis*: possible role for CFTR. *Am. J. Physiol.* 267:C491–C500.

Fischer, H., K.-M. Kreusel, B. Illek, T.E. Machen, U. Hegel, and W. Clauss. 1992. The outwardly rectifying Cl^- channel is not involved in cAMP-mediated Cl^- secretion in HT-29 cells: evidence for a very-low-conductance Cl^- channel. *Pflügers Arch.* 422:159–167.

Frizzell, R.A., G. Rechkemmer, and R.L. Shoemaker. 1986. Altered regulation of airway epithelial cell chloride channels in cystic fibrosis. *Science.* 233:558–560.

Gögelein, H., E. Schlatter, and R. Greger. 1987. The "small" conductance chloride channel in the luminal membrane of the rectal gland of the dogfish (*Squalus acanthias*). *Pflügers Arch.* 409: 122–125.

Gray, M.A., A. Harris, L. Coleman, J.R. Greenwell, and B.E. Argent. 1989. Two types of chloride channel on duct cells cultured from human fetal pancreas. *Am. J. Physiol.* 257:C240–C251.

Gray, M.A., C.E. Pollard, A. Harris, L. Coleman, J.R. Greenwell, and B.E. Argent. 1990. Anion selectivity and block of the small-conductance chloride channel on pancreatic duct cells. *Am. J. Physiol.* 259:C752–C761.

Greger, R. 1996. The membrane transporters regulating epithelial NaCl secretion. *Pflügers Arch.* 432:579–588.

Greger, R., E. Schlatter, and H. Gögelein. 1987. Chloride channels in the luminal membrane of the rectal gland of the dogfish (*Squalus acanthias*). Properties of the "larger" conductance channel. *Pflügers Arch.* 409:114–121.

Greger, R., E. Schlatter, F. Wang, and J.N. Forrest, Jr. 1984. Mechanism of NaCl secretion in rectal gland tubules of spiny dogfish (*Squalus acanthias*). III. Effects of stimulation of secretion by cyclic AMP. *Pflügers Arch.* 402:376–384.

Haws, C., M.E. Krouse, Y. Xia, D.C. Gruenert, and J.J. Wine. 1992. CFTR channels in immortalized human airway cells. *Am. J. Physiol.* 263:L692–L707.

Hayslett, J.P., H. Gögelein, K. Kunzelmann, and R. Greger. 1987. Characteristics of apical chloride channels in human colon cells (HT29). *Pflügers Arch.* 410:487–494.

Jovov, B., I.I. Ismailov, B.K. Berdiev, C.M. Fuller, E.J. Sorscher, J.R. Dedmon, M.A. Kaetrel, and D.J. Benos. 1995. Interaction between cystic fibrosis transmembrane conductance regulator and outwardly rectified chloride channels. *J. Biol. Chem.* 270:29194–29200.

Koefoed-Johnsen, V., H.H. Ussing, and K. Zerahn. 1952. The origin of the short-circuit current in the adrenalin-stimulated frog skin. *Acta Physiol. Scand.* 27:38–48.

Kunzelmann, K., M. Grolik, R. Kubitz, and R. Greger. 1992. cAMP-

dependent activation of small-conductance Cl^- channels in HT29 colon carcinoma cells. *Pflügers Arch.* 421:230–237.

Kunzelmann, K., T. Koslowski, T. Hug, D.C. Gruenert, and R. Greger. 1994. cAMP-dependent activation of ion conductances in bronchial epithelial cells. *Pflügers Arch.* 428:590–596.

Larsen, E.H., E.M. Price, S.E. Gabriel, M.J. Stutts, and R.C. Boucher. 1996. Clusters of Cl^- channels in CFTR-expressing *Sf*9 cells switch spontaneously between slow and fast gating modes. *Pflügers Arch.* 432:528–537.

Linsdell, P., and J.W. Hanrahan. 1996*a*. Flickery block of single CFTR chloride channels by intracellular anions and osmolytes. *Am. J. Physiol.* 271:C628–C634.

Linsdell, P., and J.W. Hanrahan. 1996*b*. Disulphonic stilbene block of cystic fibrosis transmembrane conductance regulator Cl^- channels expressed in a mammalian cell line and its regulation by a critical pore residue. *J. Physiol. (Camb.)*. 496:687–693.

Linsdell, P., J.A. Tabcharani, and J.W. Hanrahan. 1997. Multi-ion mechanism for ion permeation and block in the cystic fibrosis transmembrane conductance regulator chloride channel. *J. Gen. Physiol.* 110:365–377.

Lohrmann, E., and R. Greger. 1993. Isolated perfused rabbit colon crypts: stimulation of Cl^- secretion by forskolin. *Pflügers Arch.* 425:373–380.

McCarty, N.A., S. McDonough, B.N. Cohen, J.R. Riordan, N. Davidson, and H.A. Lester. 1993. Voltage-dependent block of the cystic fibrosis transmembrane conductance regulator Cl^- channel by two closely related arylaminobenzoates. *J. Gen. Physiol.* 102:1–23.

Mills, J.W., and B.E. Prum. 1984. Morphology of the exocrine glands of the frog skin. *Am. J. Anat.* 171:91–106.

Mills, J.W., K. Thurau, A. Doerge, and R. Rick. 1985. Electron microprobe analysis of intracellular electrolytes in resting and isoproterenol-stimulated exocrine glands of frog skin. *J. Membr. Biol.* 86:211–220.

Neher, E. 1992. Corrections for liquid junction potentials in patch clamp experiments. *Methods Enzymol.* 207:123–131.

Overholt, J.L., M.E. Hobert, and R.D. Harvey. 1993. On the mechanism of rectification of the isoproterenol-activated chloride current in guinea-pig ventricular myocytes. *J. Gen. Physiol.* 102:871–895.

Overholt, J.L., A. Saulino, M.L. Drumm, and R.D. Harvey. 1995. Rectification of whole cell cystic fibrosis transmembrane conductance regulator chloride current. *Am. J. Physiol.* 268:C636–C646.

Petersen, O.H. 1992. Stimulus-secretion coupling: cytoplasmic calcium signals and the control of ion channels in exocrine acinar cells. *J. Physiol. (Camb.)*. 448:1–51.

Price, M.P., H. Ishihara, D.N. Sheppard, and M.J. Welsh. 1996. Function of *Xenopus* cystic fibrosis transmembrane conductance regulator (CFTR) Cl^- channels and use of human-*Xenopus* chimeras to investigate the pore properties of CFTR. *J. Biol. Chem.* 271:25184–25191.

Schultz, B.D., A.D.G. DeRoos, C.J. Venglarik, A.K. Singh, R.A. Frizzell, and R.J. Bridges. 1996. Glibenclamide blockade of CFTR chloride channels. *Am. J. Physiol.* 271:L192–L200.

Schwiebert, E.M., T. Flotte, G.R. Cutting, and W.B. Guggino. 1994. Both CFTR and outwardly rectifying chloride channels contribute to cAMP-stimulated whole cell chloride currents. *Am. J. Physiol.* 266:C1464–C1477.

Shen, B.-Q., R.J. Mrsny, W.E. Finkbeiner, and J.H. Widdicombe. 1995. Role of CFTR in chloride secretion across human tracheal epithelium. *Am. J. Physiol.* 269:L561–L566.

Sheppard, D.N., and K.A. Robinson. 1997. Mechanism of glibenclamide inhibition of cystic fibrosis transmembrane conductance regulator Cl^- channels expressed in a murine cell line. *J. Physiol. (Camb.)*. 503:333–346.

Sokal, R.R., and F.J. Rohlf. 1981. Biometry. The principles and practice of statistics in biological research. 2nd edition. W.H. Freeman & Co., New York. 671–677.

Sørensen, J.B., and E.H Larsen. 1997. Whole-cell patch-clamp studies of exocrine glands from frog skin (*Rana esculenta*). *FASEB J.* 11:*A*306. Abstr.

Sørensen, J.B., and E.H. Larsen. 1998*a*. Co-existence of Cl^- and Na^+ channels in the apical membrane of exocrine gland acini (*Rana esculenta*). *J. Physiol.* (*Camb.*). 507.P:2P. (Abstr.)

Sørensen, J.B., and E.H. Larsen. 1998*b*. Single-channel properties of Cl^- channels from the luminal membrane of frog skin glands (*Rana esculenta*). *Pflügers Arch.* 435S:R53.

Sørensen, J.B., M.S. Nielsen, R. Nielsen, and E.H. Larsen. 1998. Luminal ion channels involved in isotonic secretion by Na^+-recirculation in exocrine gland-acini. *Biol. Skr. Dan. Vid. Selsk.* 49:166–178.

Tabcharani, J.A., X.-B. Chang, J.R. Riordan, and J.W. Hanrahan. 1991. Phosphorylation-regulated Cl^- channel in CHO cells stably expressing the cystic fibrosis gene. *Nature.* 352:628–631.

Tabcharani, J.A., X.-B. Chang, J.R. Riordan, and J.W. Hanrahan. 1992. The cystic fibrosis transmembrane conductance regulator chloride channel. Iodide block and permeation. *Biophys. J.* 62:1–4.

Tabcharani, J.A., P. Linsdell, and J.W. Hanrahan. 1997. Halide permeation in wild-type and mutant cystic fibrosis transmembrane conductance regulator chloride channel. *J. Gen. Physiol.* 110:341–354.

Thompson, I.G., and J.W. Mills. 1983. Chloride transport in glands of frog skin. *Am. J. Physiol.* 244:C221–C226.

Ussing, H.H., F. Lind, and E.H. Larsen. 1996. Ion secretion and isotonic transport in frog skin glands. *J. Membr. Biol.* 152:101–110.